Supporting Information

Gerardin et al. 10.1073/pnas.1006285107

SI Methods

Observers. Seven students from the University of Birmingham, United Kingdom, participated in this study. All observers had normal or corrected to normal vision and all were right-handed. The study was approved by the local ethics committee and all participants gave written informed consent.

Stimuli. The stimuli were created with Matlab 7.1 (Mathworks), and displayed with the PsychToolbox (1, 2). All stimuli (8 × 8°) were created in greyscale. Bright (42 cd/m^{-2}) and dark (1 cd/m^{-2}) contours defined a ring displayed on a gray background (21 cd/m^{-2}). All displays used in this study were gamma-corrected in luminance. Each ring was divided in eight equal sectors (of 45° each) and all but one had the same appearance (i.e., convex or concave). The light source was simulated at a position of ±22.5° or ±67.5° away from the vertical meridian (Fig. 1B).

The perception of concavity or convexity in combination to the light source direction (left or right and ± 22.5 or 67.5°) produces eight types of images (Fig. 1A). The odd sector could be located at any of six positions shown in Fig. 1A, image "a." Note that, apart from the odd sector, the eight images shown in this figure are the results of rotating the first image (Fig. 1A, image "a") in steps of 45°. The stimuli were blurred by applying low-pass filters to enhance depth perception. To avoid a perceptual bias for convex stimuli found in our previous study (3) when blur increased, we chose two Gaussian filters with small SDs (either 2.82 or 4.00 pixels). As a result, no differences in correct responses were found between convex and concave stimuli (Fig. S1B). Once the filter was applied, the image contrast was readjusted to cover the full range. All together, 96 stimuli were created and shown to all observers, corresponding to two shapes (convex and concave), four light directions (±22.5 and ±67.5°), six odd sector positions (three on the left, three on the right), and two blur levels.

Procedure. For each individual observer, we identified cortical areas involved in the processing of 3D shape-from-shading. We presented observers with 48 ring stimuli [two shapes (convex or concave) × four light directions (±22.5° and ±67.5°) × six sector positions] and 24 scrambled versions of these stimuli. Observers were instructed to perform a detection task on the fixation (i.e., participants were asked to press a button when the fixation cross changed from "+" to "×"). Each observer was tested in four scanning runs. Each run consisted of 18 blocks plus four fixation intervals (including one at the start, one at the end, and one between each repetition) and lasted for 352 s. We tested six conditions: left-lit convex, left-lit concave, right-lit convex, right-lit concave, scrambled convex, and scrambled concave stimuli. Each block comprised stimuli (n = 12) of one condition and it was repeated three times. Blocks were presented in a randomized sequence. Each stimulus was presented for 200 ms followed by a blank interval (600 ms).

To investigate whether neural populations in these regions reflect biases in the perception of shape-from-shading, we presented the same stimulus using eight image types (two shapes by four light directions). Each observer participated in eight scanning runs. Each run consisted of 18 blocks and two fixation intervals (one at the beginning, one at the end) and lasted 288 s. The eight image types (Fig. 1B) were repeated randomly two times in each scan. Each image type (equaling six stimuli for the odd sector locations) defined one block. Each stimulus was presented for 200 ms and followed by a blank (600 ms). To ensure that our results could not be explained by attentional differences, during all functional MRI

(fMRI) experiments, observers were instructed to detect a change in the orientation of the fixation cross ("×" turned "+"). Performance for this task was 82% correct (±2%) for the first fMRI experiment (ring stimuli vs. scrambled) and 80% (±3%) for the second (eight image types).

Mapping Regions of Interest. For each observer we identified: (i) retinotopic areas, (ii) the lateral occipital complex (LOC), (iii) motion-related areas (V3B/KO, hMT+/V5), and (iv) shape-from-shading responsive areas. We localized retinotopic areas using standard mapping procedures (4–6). We localized the LOC, V3B/KO, and hMT+/V5 using the general linear model, including fixation periods and movement correction parameters as covariates of no interest. The LOC was defined as the set of contiguous voxels in the ventral occipito-temporal cortex that showed significantly stronger activation [t(165) > 4.0, P < 0.001] for intact than scrambled images (7). The hMT+/V5 (8) was defined as the set of contiguous voxels in the lateral occipito-temporal cortex that showed significantly stronger activation [t(165) > 4.0, P < 0.001] for moving than static random dots. The V3B/KO was defined as the set of contiguous voxels anterior to V3A that showed significantly stronger activation [t(165) > 4.0, P < 0.001] for random-dot displays that defined relative than transparent motion (9). To identify cortical regions responsive to shape-from-shading, we compared fMRI responses to the ring stimuli and scrambled versions of the stimuli using the general linear model. We performed this analysis across the group of subjects and for each individual observer. For the group analysis, smoothed volume time-course data (Gaussian kernel of 6 mm FWHM) was z-transformed and modeled with six regressors of interest [six stimulus conditions (four light orientations and two scrambled) and fixation baseline] convolved with a canonical hemodynamic response function.

SI Results

Psychophysical Results. Because the images are ambiguous (a convex shape lit from below produces the same image as a concave shape lit from above), there is no correct answer for the perceived shape of the odd element in our psychophysical task. Therefore, the proper way to display what the observers perceive is to report the proportion of times convexity is perceived for each image type, as we have done in Fig. 1C. However, it is still informative to look at our psychophysical data if we assume that the light source is above. In this case, image types "a," "b," "g," and "h" from Fig. 1A correspond to convex rings, and image types "c," "d," "e," and "f" to concave rings (see Fig. 1B). Fig. S1A represents the percentage of correct responses under this assumption for the four lighting directions. The plot shows a maximum for stimuli from the left at −22.5°, which is consistent with the claim that observers had a bias to the left for the assumed light source position. In contrast, stimuli lit from the right at 67.5° were significantly different [F(1,12) = 35.9, P < 0.0001] and produced performance close to chance.

Fig. S1B represents the percentage of correct responses when the data are pooled across object shape (Upper) or across global lighting direction (Lower). Again, assuming above illumination, convex scores are percent-correct for reporting a concave odd sector in a globally convex stimulus (and similarly for concave scores). There are no differences between concave and convex scores [F(1,54) = 0.91, P = 0.34], indicating that our stimuli did not generate a biased response in favor of one of the two shapes. This lack of bias for convex shapes was desired (to avoid a potential confound) and expected from the choice of the low-pass filters applied on the images (see our previous study in ref. 3).

Finally, again assuming above illumination, left scores are percent-correct for correctly reporting the shape of the odd sector when the object is lit from the left side (and similarly for right scores). Left scores are consistently larger than right scores [$F_{(1,54)} = 22.09$, $P < 0.0001$], indicating observers reported a perceived shape that agreed better with the light-from-above assumption when the object was lit from the left. This advantage for left scores comes from the bias to the left for the assumed light-source position, and as such is another measure of the left bias of each observer.

Behavior Classifier Models. We detail here the simple models we used to determine the expected accuracy performance of the Shape and Light behavior classifiers. The Shape behavior model uses the behavioral data for each observer (Fig. 1C) to determine the reliability of the shape judgment of each image. More precisely, it represents the reliability with which an image is judged as a convex ring with a normal distribution centered on the proportion of convex judgments of that image (say around 80% for image "a") and with SD the SE of these judgments scaled by a noise factor. This scaling noise factor could represent a mixture of the noise inherent in the fMRI signal collection and the fact that our classifier used at most 100 voxels, whereas the observer as a whole has access potentially to the output of many more cells in an area. The value chosen for the scaling factor (constant for all images) did not change the pattern of performance across the four classifiers, so we decided to set it separately for each observer so that the maximum model performance matched the best classifier performance found across any cortical area for that observer.

Each classifier (e.g., the second one in Fig. 3A) therefore has access to two distributions representing the convexity strength of the two images to classify (images "a" and "e" for the second classifier). From Signal Detection Theory (10), the sensitivity to classify these two images is represented by the distance between the means of the distributions normalized by the SD of the distributions. Intuitively, classification performance increases the further apart the two distributions are and the less spread there is around the means. Therefore, there are two factors that can affect the classification accuracy, the difference in shape judgment between the images and the variability of the decisions. Classification accuracy will deteriorate with higher perceptual similarity between the two images and higher variability in the perceptual judgments.

The Light behavior model uses the behavioral data for each observer to determine the bias to the left for the assumed light source position from the shift of the scaled cosine of the fit of the shape judgments (Fig. 1C). More precisely, it represents the prior distribution for light directions as a von Mises distribution (the generalization of the normal distribution for circular variables) with mean equal to the measured bias. We then assume that the information in the image about light direction is unbiased and can thus be represented by another von Mises distribution, with mean equal to the simulated light direction. Prior and likelihood are combined using Bayes' rule to produce a posterior distribution that represents the relative evidence that a particular image is lit from one direction or another. The Light behavior model takes the mean of the posterior distribution as the estimate of the light source for that image, and the variance of that distribution as a measure of uncertainty of that estimate. These light estimates are biased toward the mean of the prior: that is, toward the above-left. We can thus compute the performance of our Light behavior model that attempts to classify pairs of images using the same Signal Detection Theory principles that we used for the Shape behavior model (see above). More precisely, the performance of the Light behavior model was estimated from the distance between the means of light estimates normalized by the SD of the estimates.

So far, we have neglected to discuss the concentration parameters (the equivalent of the inverse of the variance for von Mises distributions) of the prior and likelihood functions. We first assume that the concentration parameter of the likelihood is identical for all light directions (a reasonable assumption given that the likelihood represents the information in the image and that this information does not change when one rotates the image). Then we note that the actual values of the concentration parameters for the likelihood and prior do not change the ordering of the performance for the four pairs of images submitted to the classifier, they only change the overall mean performance of the classifiers and the magnitude of the difference between the classifiers. Because we are only interested in the order of the performance of the four classifiers (we use Spearman correlations to match these models to the classifiers for each region in Fig. 5B), we have adjusted the concentration parameters so that the maximum performance of our model (for the "b–g" comparison) was identical to the best performance of any brain area. The performance of the Light behavior model is shown in Fig. 4C. Note that this performance is an asymmetric U-shape with respect to the four comparisons, the asymmetry resulting from the left bias for the estimated light direction.

Control Analyses for the Multivoxel Pattern Analysis Results. We conducted several additional analyses to control for possible confounds. First, multivoxel pattern analysis (MVPA) on univariate signals from the same regions of interest (average signal across voxels) showed that information about Shape classification could not be reliably extracted from the average signal across voxels, supporting the advantage of MVPA in decoding shape from shading from brain patterns across voxels. Second, we ran the same classifiers with randomly assigned category labels to the activation patterns. Accuracies were not significantly different from chance, suggesting that the classification results could not be attributed to random patterns in the data. Third, analysis of the functional signal-to-noise ratio showed no significant differences across areas (Fig. S2), suggesting that differences in the MVPA results across areas could not be simply attributed to differences in the fMRI signals across areas. Comparison of MVPA and control analyses for selected areas [V3B/KO, lateral occipital (LO), ventral intraparietal sulcus (VIPS), parieto-occipital intraparietal sulcus (POIPS)] is shown in Table S3. Finally, our MVPA results could not be significantly confounded by differences in the attentional state of the observers or eye movements across conditions. During scanning, observers performed a fixation task (i.e., they were instructed to detect a change at the fixation point) with no significant difference in performance across stimulus conditions, ensuring similar attention across all stimulus conditions. Eye-movement recordings during scanning showed that there were no significant differences in the eye position, number and amplitude of saccades across stimulus conditions (Fig. S3).

Control analyses for the Light classifiers, similar to those reported for the Shape classifiers, (Table S4) were conducted to ensure that the classification accuracies observed could not be a result of random statistical regularities in the data (shuffling) or extracted from average signals across voxels (univariate analysis).

Image-Based Correlation. Could the performance of the Shape and Light classifiers simply be explained by the pixel luminance difference between the stimuli, in other words without any reference to the observer's behavior? To address this question, we computed the cross-correlations between the pairs of images that form the bases of the classifiers: for example, the pair of images "b" and "f" for the first Shape classifier. Because the odd element could be in one of six positions, we considered all of the possible paired combinations (i.e., odd element in position i in image "b" with odd element in position j in image "f"). Across all these combinations, the mean correlation of the Shape classifier was –0.506, –0.494, –0.494, and –0.506 for classifiers 1 through 4 (Fig. 3A). The negative cor-

relations reflect the fact that white contours became black (and reversely) when a convex shape was compared with a concave one for the Shape classifier. More importantly, there was very little variability across the four Shape classifiers, thereby indicating that the pattern of performance revealed by our Shape behavior model (Fig. 3C) is the consequence of the observers' perception rather than simply some luminance asymmetry in the stimuli.
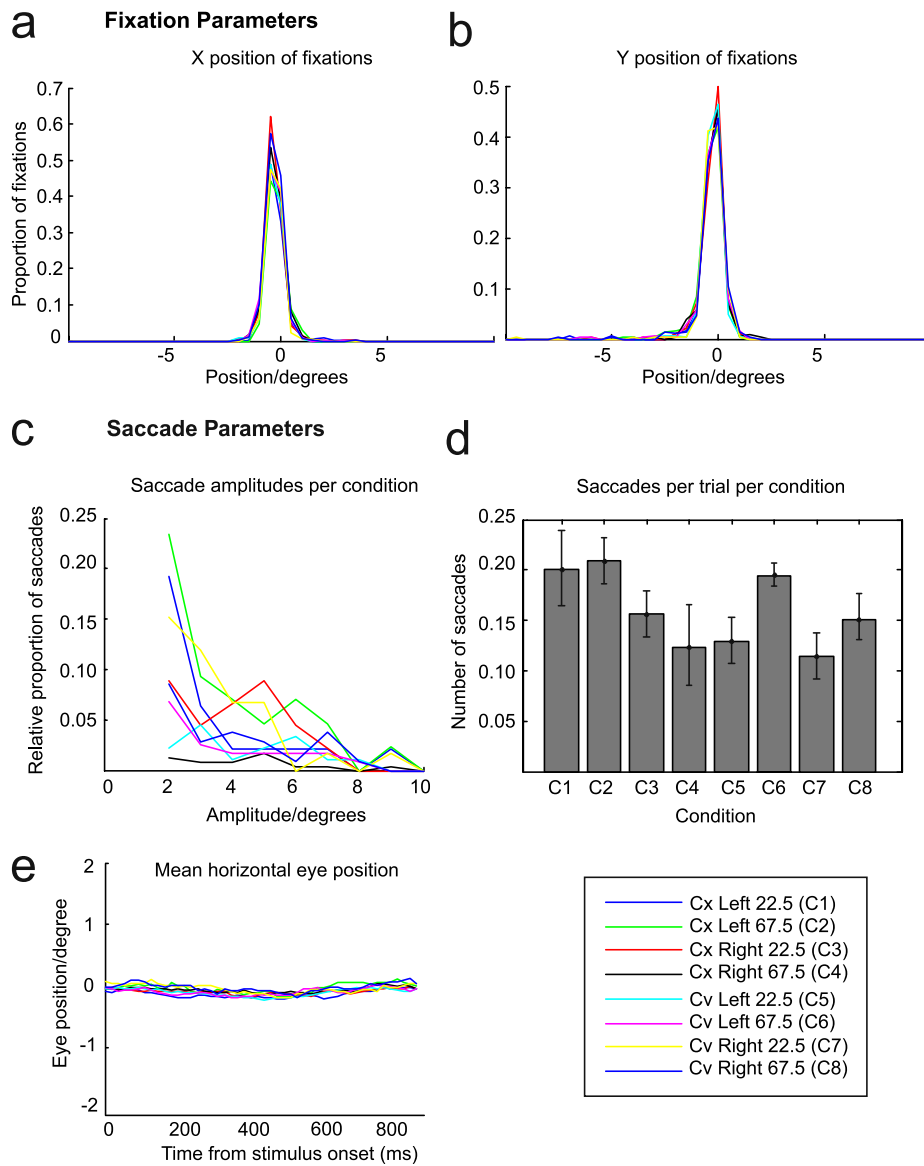
Similarly, we computed the cross-correlations across all possible paired combinations relevant to the Light classifiers: for example, the pair of images "b" and "g" for the first Light classifier. The mean correlation of the Light classifier was –0.093, 0.247, 0.247, and –0.093 for classifiers 1 through 4 (Fig. 4A). The positive correlations reflect the fact that some image pairs were quite similar (e.g., images "a" and "h"), and the near-zero correlations reflect the fact that about half of the pixels retained their contrast polarity (black or white), whereas the other half inverted their contrast (e.g., images "b" and "g"). More importantly, the pattern of correlations was symmetric across the four classifiers (i.e., performance of classifier 1 equals that of classifier 4, and classifier 2 equals classifier 3), thereby indicating that the

unbalance of our Light behavior model (Fig. 4C) is the consequence of the observer's perception rather than simply some luminance aspects of the stimuli.

Although all of the necessary information about image-pair similarity is contained in these correlation coefficients, we transformed these correlation coefficients into a performance value (proportion correct) for easier comparison with our behavior-based models. This transformation involves a model that attempts to discriminate two images that are noisy versions of two templates, templates that are more or less correlated. For the same level of noise, discrimination performance will be at chance if the two templates are perfectly correlated, and performance will increase as the correlation decreases. Note that the relationship between correlation and performance is monotonically decreasing, so the ordering of performance is not affected by the level of noise actually chosen (only the ordering is relevant for the Spearman rank correlations used to generate Fig. 5B). The outcome of these simulations was used to generate Figs. 3B (Shape Image Model) and 4B (Light Image Model) in the article.

1. Brainard DH (1997) The Psychophysics Toolbox. *Spat Vis* 10:433–436.
2. Pelli DG (1997) The VideoToolbox software for visual psychophysics: Transforming numbers into movies. *Spat Vis* 10:437–442.
3. Gerardin P, de Montalembert M, Mamassian P (2007) Shape from shading: New perspective from the Polo Mint stimulus. *J Vis* 7(11):13, 1–11.
4. Engel SA, et al. (1994) fMRI of human visual cortex. *Nature* 369:525.
5. Sereno MI, et al. (1995) Borders of multiple visual areas in humans revealed by functional magnetic resonance imaging. *Science* 268:889–893.
6. DeYoe EA, et al. (1996) Mapping striate and extrastriate visual areas in human cerebral cortex. *Proc Natl Acad Sci USA* 93:2382–2386.
7. Kourtzi Z, Kanwisher N (2001) Representation of perceived object shape by the human lateral occipital complex. *Science* 293:1506–1509.
8. Tootell RB, et al. (1995) Functional analysis of human MT and related visual cortical areas using magnetic resonance imaging. *J Neurosci* 15:3215–3230.
9. Dupont P, et al. (1997) The kinetic occipital region in human visual cortex. *Cereb Cortex* 7:283–292.
10. Green DM, Swets JA (1966) *Signal Detection Theory and Psychophysics* (Wiley, New York).

a All Subjects (N = 7)

b Performances for each Subject (N = 7)

Fig. S1. Performance under the above illumination assumption. (*A*) With the assumption that light comes from above, each image type from Fig. 1*A* is assigned a particular shape (convex or concave ring). This plot shows the performance of the observers under this assumption for the four lighting directions. The asymmetry of the plot is a signature of the bias to the left for the assumed light source position. (*B*) Comparison of performance for different shapes of the odd element and different global lighting directions. There are no biases to report convex rather than concave shapes (*Upper*) but a consistent advantage for left illuminations. Each symbol represents one observer (*n* = 7).

Fig. S2. Functional signal-to-noise ratio is shown across all regions of interest (ROIs) for responses to stimuli in the main experiment. We computed the average functional signal-to-noise ratio for the voxels included in the multivariate analysis by taking the difference between the mean response to the stimuli and the mean response to the fixation, divided by the SD of the mean across all stimulus conditions and fixation. Error bars indicate SEM across observers.

Fig. S3. Eye movements were recorded from three participants during the main experiment using the ASL 6000 videographic eye tracker (Applied Science Laboratories). Eye tracking data were preprocessed using the Eyenal software (Applied Science Laboratories) and analyzed using custom Matlab (Mathworks) software. We computed (*A*) horizontal eye position, (*B*) vertical eye position, (*C*) proportion of saccades for each condition at different saccade amplitude ranges, (*D*) number of saccades per trial per condition, and (*E*) the mean horizontal eye position. For each condition, plots of the horizontal and vertical eye positions for each stimulus type peaked and were centered on the fixation at 0°. A repeated-measurement ANOVA indicated that there was no significant difference between stimulus conditions on mean horizontal eye position [$F_{(7, 84)} = 0.63$, $P = 0.575$], mean vertical eye position [$F_{(7, 84)} = 0.877$, $P = 0.625$], mean saccade amplitude [$F_{(7, 84)} = 1.46$, $P = 0.9$], or the number of saccades per trial per condition [$F_{(7, 11)} = 3.4$, $P = 0.19$]. These results suggest that it is unlikely that our results were significantly confounded by eye movements.
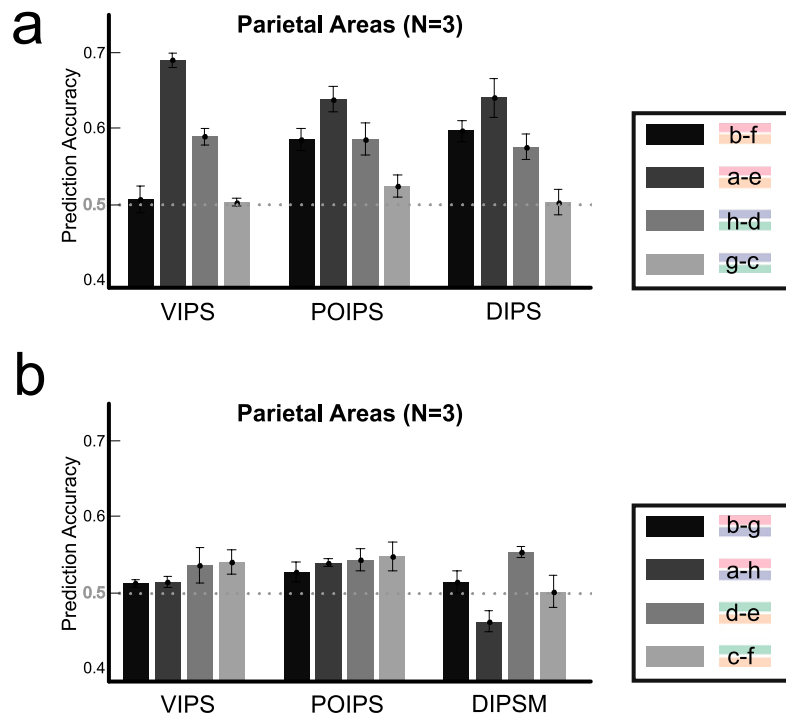
Fig. S4. (*A*) Shape classification (convex vs. concave) based on the assumed left (22.5° and 67.5°) and right (22.5° and 67.5°) light sources position [VIPS, POIPS, and dorsal intraparietal sulcus (DIPS): *n* = 3]. Prediction accuracy for the convex and concave classification across the assumed four light-source positions. Mean classification accuracy (pattern size = 100 voxels per area) across participants is shown for each ROI; error bars indicate SEM across observers. The dashed line indicates the chance classification level (50%). A significant main effect of light orientation was found for all these areas [VIPS: $F_{(3,24)}$ = 90.6, P < 0.0001; POIPS: $F_{(3,24)}$ = 25.5, P < 0.0001; and DIPS: $F_{(3,24)}$ = 34, P < 0.0001]. (*B*) Light classification (left vs. right) for the four classifiers of Fig. 4*A* across three subregions of the IPS (VIPS, POIPS and DIPS: *n* = 3). Prediction accuracy for the convex and concave classification across the assumed four light-source positions. No significant main effect of light orientation was found in these areas [VIPS: $F_{(3,24)}$ = 2.39, P = 0.09; POIPS: $F_{(3,24)}$ = 0.9, P = 0.4; and DIPS: $F_{(3,24)}$ = 0.05, P = 0.06].

Table S1. Tables of Talairach coordinates for ROI (group analysis; *n* = 7) for all areas showing significantly stronger activation for the ring stimuli vs. scrambled stimuli

PoloMint localizer	LH			RH		
ROI	x	y	z	x	y	z
LO	−39	−64	−5	44	−57	−8
V3B/KO	−34	−78	13	36	−77	13
VIPS	−24	−68	28	26	−67	27
POIPS	−20	−67	43	20	−60	44
DIPSM	−25	−52	55	20	−54	51
DIPSA				34	−40	44
PMv				46	0	27
SPL	−20	−57	56	21	−55	59
Postcentral	−52	−24	38			

LH, left hemisphere; RH, right hemisphere; LO, lateral occipital; V3B/KO, kinetic occipital, VIPS: ventral intraparietal sulcus; POIPS, parieto-occipital intraparietal sulcus; DIPS, dorsal intraparietal sulcus median (M) and anterior (A); PMv, premotor ventral; SPL, superior parietal lobule; Postcentral area. Individual analysis: only three subjects showed sufficient amount of selected voxels (>50) to run the classifiers in areas VIPS, POIPS, and DIPS (see Fig. S4).

Table S2. Effects of light directions on classifiers performance

	Shape classification			Light classification	
Areas	F(3,24)	P	Areas	F(3,24)	P
V1	2.33	0.08	V1	170.6	**<0.0001**
V2	61.67	**<0.001**	V2	164	**<0.0001**
V3v	8.09	0.054	V3v	103.8	**<0.0001**
V4v	9.13	0.084	V4v	24.1	**<0.001**
LO	55.79	**<0.0001**	LO	2.78	0.08
V3d	26.22	**<0.0001**	V3d	184.9	**<0.0001**
V3A	28.74	**<0.0001**	V3A	75.45	**<0.0001**
V7	24.18	**<0.0001**	V7	38.2	**<0.0001**
V3B/KO	51.19	**<0.0001**	V3B/KO	64.8	**<0.0001**
hMT+/V5	52.49	**<0.0001**	hMT+/V5	3.56	**<0.05**
IPS	34.02	**<0.0001**	IPS	0.18	0.9

Repeated-measures ANOVAs were performed on individual cortical areas to test the main effects of the four light directions on the classification accuracies obtained in the MVPA on Shape and Light. The table shows the F-ratios and associated P values.

Table S3. Comparison of multivariate, univariate, and shuffling analysis for representative areas: Shape

Hemispheres	All				Left				Right			
V3b/KO												
Light Source (MVPA rule)	L67	L22	R22	R67	L67	L22	R22	R67	L67	L22	R22	R67
ROC: multivariate	54.90	64.70	57.80	58.60	51.20	56.60	66.80	55.40	54.40	68.20	52.40	59.90
ROC: univariate	41.30	53.60	56.50	49.80	48.08	48.80	52.00	51.90	47.00	53.05	55.90	55.80
ROC: shuffle	48.00	49.10	48.00	50.00	48.00	52.50	51.80	51.80	53.00	51.65	49.35	50.65
LO												
Light Source (MVPA rule)	L67	L22	R22	R67	L67	L22	R22	R67	L67	L22	R22	R67
ROC: multivariate	52.00	58.80	62.20	55.60	49.30	59.00	64.50	56.00	50.80	54.60	65.10	59.00
ROC: univariate	45.60	55.90	51.30	47.00	50.70	50.70	50.25	56.00	46.00	55.70	53.80	51.75
ROC: shuffle	48.00	50.50	49.15	52.45	51.50	52.00	48.00	50.75	49.00	51.30	49.00	50.65
VIPS												
Light Source (MVPA rule)	L67	L22	R22	R67	L67	L22	R22	R67	L67	L22	R22	R67
ROC: multivariate	50.30	68.75	58.70	50.00	47.00	65.30	64.60	44.40	58.00	65.30	52.30	50.00
ROC: univariate	49.20	48.00	45.00	52.20	49.35	53.40	54.00	49.00	49.00	55.50	50.50	52.70
ROC: shuffle	53.45	50.40	51.30	50.35	54.80	52.70	48.65	49.70	48.00	51.15	50.52	51.40
POIPS												
Light Source (MVPA rule)	L67	L22	R22	R67	L67	L22	R22	R67	L67	L22	R22	R67
ROC: multivariate	58.30	63.50	58.30	52.00	52.30	68.75	42.70	46.90	56.25	60.40	57.30	51.00
ROC: univariate	50.00	52.00	48.00	48.00	48.00	55.20	47.90	53.50	49.15	51.30	49.70	55.50
ROC: shuffle	53.50	51.50	51.00	52.00	53.40	50.60	49.15	49.40	52.80	50.45	49.55	51.55

Shape classification (convex, concave) according to each light source position (left or right 67.5° and 22.5°).

Table S4. Comparison of multivariate, univariate, and shuffling analysis for representative areas: Light

Hemispheres	All				Left				Right			
V1												
Light Source (MVPA rule)	Cx67	Cx22	Cv22	Cv67	Cx67	Cx22	Cv22	Cv67	Cx67	Cx22	Cv22	Cv67
ROC: multivariate	64.10	56.70	46.80	61.20	56.80	56.00	50.70	59.70	63.30	54.70	48.00	65.80
ROC: univariate	53.60	50.35	50.00	52.00	49.00	51.00	49.50	49.30	50.00	49.50	49.15	50.65
ROC: shuffle	52.70	51.30	51.00	52.80	52.00	48.30	51.30	54.50	46.35	52.40	53.70	49.20
V3												
Light Source (MVPA rule)	Cx67	Cx22	Cv22	Cv67	Cx67	Cx22	Cv22	Cv67	Cx67	Cx22	Cv22	Cv67
ROC: multivariate	65.50	52.80	49.90	64.20	50.80	51.10	51.10	63.30	62.30	54.20	49.40	53.50
ROC: univariate	55.00	48.70	46.30	54.20	50.60	52.60	48.60	48.00	52.40	50.15	47.80	52.10
ROC: shuffle	53.40	48.00	51.50	51.20	47.75	47.80	53.20	53.00	48.20	50.00	49.50	50.65
V3A												
Light Source (MVPA rule)	Cx67	Cx22	Cv22	Cv67	Cx67	Cx22	Cv22	Cv67	Cx67	Cx22	Cv22	Cv67
ROC: multivariate	58.50	56.00	51.00	63.00	56.30	53.50	48.80	63.20	52.70	54.90	49.00	53.70
ROC: univariate	47.00	56.40	48.40	52.90	49.00	54.00	50.70	46.40	52.15	50.40	50.00	51.50
ROC: shuffle	53.00	47.00	50.70	49.60	48.00	49.0	52.00	52.20	48.90	51.30	50.80	49.30
VP												
Light Source (MVPA rule)	Cx67	Cx22	Cv22	Cv67	Cx67	Cx22	Cv22	Cv67	Cx67	Cx22	Cv22	Cv67
ROC: multivariate	64.10	55.40	49.90	55.20	50.70	48.75	45.50	53.70	57.00	54.60	50.40	57.30
ROC: univariate	47.00	52.40	50.30	52.40	50.05	49.40	49.00	48.60	54.00	52.05	51.10	50.50
ROC: shuffle	50.00	47.00	52.00	50.50	51.00	50.60	52.30	48.80	48.70	50.70	49.72	47.00

Light classification (left, right) according to each lit shape (convex or concave at 22.5° and 67°).